Nanoscale

PAPER

View Article Online
View Journal | View Issue

Cite this: *Nanoscale*, 2014, **6**, 12573

A novel upconversion, fluorescence resonance energy transfer biosensor (FRET) for sensitive detection of lead ions in human serum†

Sai Xu, Shihan Xu, Yongsheng Zhu, Wen Xu, Pingwei Zhou, Chunyang Zhou, Biao Dong and Hongwei Song*

Received 5th June 2014,
Accepted 9th August 2014

DOI: 10.1039/c4nr03092c

www.rsc.org/nanoscale

There has been great progress in the development of fluorescence biosensors based on quantum dots (QDs) for the detection of lead ions. However, most methods are detecting lead ions in aqueous solution rather than in human serum due to the influence of protein autofluorescence in serum excited by visible light. Thus, we developed a novel fluorescence resonance energy transfer (FRET) biosensor by choosing the upconversion $NaYF_4$:Yb^{3+}/Tm^{3+} nanoparticles as the energy donor and the CdTe QDs as the energy acceptor for lead ion detection. It is the first near infrared (NIR)-excited fluorescent probe for determination of lead ions in serum that is capable of overcoming self-luminescence from serum excitation with visible light. The sensor also shows high selectivity, a low detection limit (80 nm) and good linear Stern–Volmer characteristics (R = 0.996), both in the buffer and serum. This biosensor has great potential for versatile applications in lead ion detection in biological and analytical fields.

1. Introduction

Lead is one of the most toxic heavy metals, and trace amounts can harm human health even at a very low concentration of 100 ppb (480 nm); therefore, a sensitive and specific method for detecting lead ions is in high demand.[1] A variety of methods have been employed for the determination of lead ion levels in body fluids, such as blood and urine, including atomic absorption spectrometry, inductively coupled plasma mass spectrometry (ICP/MS), anodic stripping voltammetry, and electrochemical methods.[2–5] However, these methods are limited due to the necessity for sophisticated equipment and complicated retreatment of samples. The need for facile, rapid, inexpensive and highly sensitive methods for the detection of lead ions continues. To meet this need, in recent years several groups have developed novel fluorescent probes that can selectively respond to lead ions. These probes are either based on small organic luminescent dyes, metalloregulatory proteins, or DNAzymes.[6–8] Progress in developing these methods has occurred, although problems remain in applying them to biomonitoring. For instance, organic luminescent dyes are photo-bleached after continuous irradiation by ultraviolet or visible light.[9] Sensors based on nucleic acids are fragile even before complicated chemical modification due to disintegration by nucleases in body fluids.[10]

Recently, a variety of quantum dots (QDs)-based fluorescent sensors have been developed for lead ion detection with the advantages of high sensitivity, simplicity and low cost due to the attractive optical properties of QDs, including size-tunable emission profiles, high luminescence quantum efficiency, and excellent photochemical stability.[11–15] For example, Ying and coworkers developed a method for Pb^{2+} detection based on glutathione (GSH)-capped ZnCdSe QDs.[11] Tao's group investigated using the self-assembly technique to produce xylenol orange (XO)-functionalized CdSe/CdS QDs for lead ion determination.[15] These methods all exhibited excellent sensitivity due to the specific and strong affinity of ligands capped on the QDs with lead ions and the unique luminescence properties of QDs. However, all the methods mentioned here detect lead ions in aqueous solution rather than in serum. There is a fatal flaw for lead ion detection in human serum based on QDs, namely, the porphyrin, serological proteins, and carotenoids in the serum can be excited by visible light to emit in the fluorescence range from 500 to 600 nm, which can greatly influence results.[16] Consequently, challenges remain to develop facile methods for the sensitive and selective determination of lead ions, especially in human serum. To solve this problem, we developed a novel lead sensor based on fluorescence resonance energy transfer (FRET) by selecting upconversion nanoparticles (UCNPs) as the energy donor and thioglycolic acid

State Key Laboratory on Integrated Optoelectronics, College of Electronic Science and Engineering, Jilin University, 2699 Qianjin Street, Changchun 130012, China. E-mail: songhw@jlu.edu.cn

† Electronic supplementary information (ESI) available. See DOI: 10.1039/c4nr03092c

(TGA)-capped CdTe QDs as the energy acceptor. FRET is a non-radiation process characterized by energy transfer between an excited donor and an acceptor through long-range dipole–dipole interaction, which is widely used as a spectroscopic ruler in biosensing and bioimaging.[17,18] An efficient FRET process requires the following: (1) the acceptor absorption spectrum overlaps with the donor emission spectrum; and (2) the distance between a donor and an acceptor must be linked in close proximity, typically less than a few nanometers.[19] CdTe is an important semiconductor nanomaterial that demonstrates high quantum yields and has been used in numerous applications, such as in light-emitting devices, solar cells and biological labels.[20–22] Moreover, the UCNPs, which are capable of emitting strong visible luminescence under near infrared (NIR) excitation, possess various advantages due to their unique anti-Stokes fluorescence properties, such as large penetration depth into tissues, high chemical stability and low toxicity.[23] In addition, under NIR excitation, the autofluorescence from biological samples and scattering light becomes negligible. As a result, several sensors based on UC-FRET have been established in biosensing and bioimaging. Jiang and his coworkers developed a new type of Cu^{2+} sensor based on FRET between UCNPs and RB-hydrazide.[24] Similarly, a later study of the sensing and bioimaging of methylmercury by a highly sensitive water-soluble nanosystem based on cyanine dye-assembled UCNPs was reported by Li's group.[25]

In this work, a novel FRET sensor is obtained by selecting $NaYF_4$:Yb^{3+}/Tm^{3+} as the energy donor and CdTe QDs as the energy acceptor for lead ion detection. This system is expected to be used for selective and sensitive quantification of lead in serum; meanwhile, NIR excitation overcomes the self-luminescence of serum excited by visible light.

2. Experimental section

2.1. Synthesis of PEI-modified $NaYF_4$:Yb,Tm UCNPs

PEI-modified water-soluble $NaYF_4$:Yb,Tm UCNPs were synthesized *via* a solvothermal method following a procedure reported by Liu.[26] Briefly, NaCl (2.5 mmol), PEI (0.4 g), $Y(NO_3)_3$ (0.878 mmol), $Yb(NO_3)_3$ (0.12 mmol), and $Tm(NO_3)_3$ (0.002 mmol) were dissolved in ethylene glycol (15 mL) under vigorous stirring. After the solution became transparent, NH_4F (4 mmol) in ethylene glycol (10 mL) was dropwise added to the solution under vigorous stirring. After stirring for another 10 min, the entire mixture solution was transferred into a 25 mL Teflon-lined stainless steel autoclave. The autoclave was sealed and heated under 200 °C for 4 h. After the autoclave had cooled to room temperature naturally, $NaYF_4$:Yb,Tm UCNPs were collected by centrifugation and washed with deionized water and alcohol three times.

2.2. Synthesis of TGA-capped CdTe QDs

Briefly, 80 mg of $NaBH_4$ were transferred to a small vial; then 3 mL of ultrapure water were added. After 127.5 mg of tellurium powder were added in the vial, the reacting system was cooled by ice. During the reaction, a small outlet connected to the vial was kept open to discharge pressure from the resulting hydrogen. After approximately 8 h, the black tellurium powder disappeared and NaB_4O_7 white precipitation appeared on the bottom of the vial instead. The resulting NaHTe in the clear supernatant was separated.

A series of aqueous colloidal CdTe QDs were prepared by adding freshly prepared NaHTe solution to N_2-saturated $CdCl_2$ solutions at pH 9.0 in the presence of TGA as a stabilizing agent. After 2 days standing in the dark, the resulting mixture was subjected to 80 °C reflux for 4 h to obtain the QDs with the absorption of 480 nm.[27]

2.3. Characterization

Transmission electron micrographs were obtained with a Hitachi H-800 transmission electron microscope (TEM) operating at an acceleration voltage of 200 kV. High-resolution transmission electron microscope (HR-TEM) images were recorded on a FEI Tecnai G2 S-Twin microscope operated with an acceleration voltage of 200 kV. The crystalline structure of the samples was characterized by X-ray diffraction (XRD) (Rigaku D/max-rA power diffractometer using Cu-KR radiation (λ) 1.54178 Å). Ultraviolet-visible (UV-vis) absorption spectra were measured with a Shimadzu UV-3101PC UV-vis scanning spectrophotometer ranging of 200–1100 nm.

2.4. Detection of FRET process from UCNPs to QDs

A specified concentration of UCNPs was transferred to a cuvette, and then a different concentration of QDs was added to the solution. After a 10 min incubation at room temperature, the luminescence spectra were measured with a photomultiplier combined with a monochromator for signal collection from 400 nm to 700 nm. A continuous 980 nm diode laser was used to pump the samples to investigate steady-state spectra. In the measurements of luminescent dynamics, the samples were pumped by a laser system consisting of a Nd:YAG pumping laser (1064 nm), the third-order harmonic generator (355 nm) and a tunable optical parameter oscillator (OPO, Continuum Precision II 8000). Pulse duration was 10 ns, repetition frequency 10 Hz, and line width 4–7 cm^{-1}.

2.5. Sensitivity and selectivity of Pb^{2+} detection in PBS buffer

Lead nitrate was used for the Pb^{2+}-sensitivity studies. PEI-functioned UCNPs and TGA-capped QDs were mixed in the buffer, after a 10 min incubation at room temperature. Different Pb^{2+} concentrations were added to the mixture solution, and then luminescence spectra were measured with the same equipment described in section 2.4. To determine FRET probe selectivity, various ions, including Mg^{2+}, Ca^{2+}, Fe^{2+}, K^+, Na^+, Cl^-, Zn^{2+}, Cu^{2+}, Ni^{2+}, and Co^{2+}, were prepared at a concentration of 1 μM. The solutions above and 1 μM of Pb^{2+} solution were added to the mixture individually and changes in fluorescence were monitored.

In the control experiment, the QD solution was transferred to a cuvette, and then a specific concentration of Pb^{2+} was

added. The emission spectra were measured under 480 nm excitation with a SENS-9000 spectrometer.

2.6. Detection of Pb^{2+} in real samples

The functionalized UCNPs and QDs were incubated in the serum; after a 10 min incubation at room temperature, a different Pb^{2+} concentration was added to the mixture solution. The luminescence spectra were measured with the same equipment as the detection process in the buffer.

In the control experiment, QDs were mixed in the serum, and then a different concentration of Pb^{2+} was added; the luminescence spectra were measured with the same equipment as the detection process in the buffer.

3. Results and discussion

3.1. Morphology and structure of $NaYF_4$:Yb,Tm UCNPs and CdTe QDs

The UCNPs and QDs could be well-dispersed in water to form stable colloidal solutions directly without further surface modification, due to the presence of the PEI and TGA capped layer on their surfaces. Fig. 1(a) shows the TEM of spherical morphology of the $NaYF_4$:Yb,Tm UCNPs with an average diameter of 16 nm. The inset shows the HR-TEM of the lattice fringes with an observed d-spacing of 0.3158 nm, which is in good agreement with the lattice spacing in the (111) planes of cubic $NaYF_4$ (0.316 nm, JCPDS: 77-2042). Fig. 1(b) exhibits XRD patterns of the UCNPs. It can be seen that all peak positions and intensities can be well indexed in accordance with cubic $NaYF_4$ crystals (JCPDS: 77-2042), suggesting high product crystallinity. Fig. 1(c) shows the HR-TEM picture of the water-dispersed CdTe QDs, in which the size of pristine CdTe QDs was estimated to be ~2.6 nm. Note that the size from TEM measurement matches well with that from calculations according to its ultraviolet-visible absorption spectra. The known formula for CdTe QD size, summarized by Peng *et al.*, can be expressed as follows:[28]

$$D = (9.8127\times10^{-7})\lambda^3 - (1.7147\times10^{-3})\lambda^2 + 1.0064\lambda - 194.84 \quad (1)$$

where D (nm) is the diameter of the QDs, and λ (nm) is the absorption peak wavelength. Using eqn (1), mean QD diameter was determined to be 2.5 nm, approximately corresponding to the HR-TEM image. Fig. 1(d) demonstrates the HR-TEM image of the $NaYF_4$:Yb,Tm/CdTe QDs composites. It can be seen that the CdTe QDs were adsorbed on the surface of UCNPs; the lattice spacing of the QDs was 0.3178 nm, corresponding to the (002) planes in the hexagonal phase of CdTe QDs.

3.2. FRET process from UCNPs to QDs

Electrostatic interaction between the positively charged $-NH_3^+$ groups of the PEI-UCNPs (ζ potential = +37.2 mV) and negatively charged $-COO^-$ groups attached on the QDs (ζ potential = −18.0 mV) played the key role in formation of the FRET probe PEI-UCNPs/TGA-QDs (ζ potential = −2.46 mV). Strong attachment of CdTe QDs on the surface of UCNPs can happen by electrostatic interaction during simple mixing.

Fig. 2(a) shows the upconversion emission spectrum of $NaYF_4$:Yb,Tm nanoparticles under 980 nm excitation (blue line), absorption (red dashed line) and emission (green solid line) spectra of the QDs. The UCNPs give dual emission bands in blue and red parts of the visible region; the blue emissions are derived from $^1D_2$–$^3F_4$ (457 nm) and $^1G_4$–$^3H_6$ (484 nm) transitions of Tm^{3+}, the lines within the red region are attributed to the transition of $^1G_4$–$^3F_4$ (653 nm). The central wavelength of the absorption band of the QDs locates at 504 nm, which partly overlaps with the 457 nm and 484 nm emissions of Tm^{3+} ions. The emission band of the QDs located at 550 nm does not overlap with the emission of Tm^{3+} ions. The QD emission originates from the radiation recombination of electrons and holes trapped in defect (surface) states.[29] There are

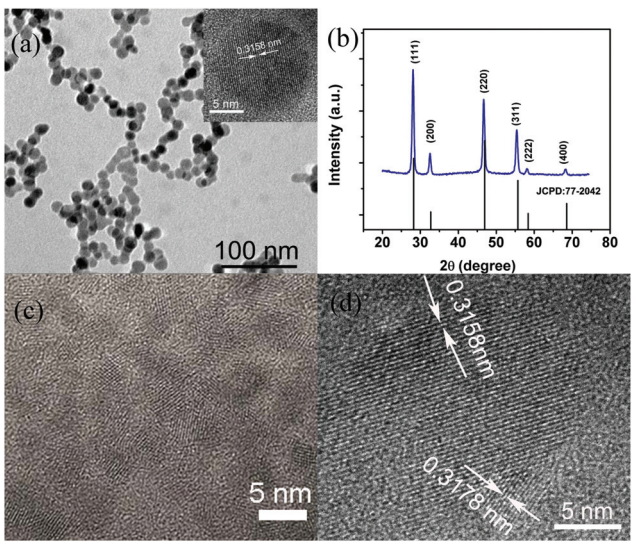

Fig. 1 (a) TEM of PEI-$NaYF_4$:Yb,Tm (inset: HR-TEM showing lattice fringes). (b) XRD patterns of the $NaYF_4$:Yb,Tm UCNPs in contrast to standard card for cubic phase $NaYF_4$. (c) HR-TEM images of pristine CdTe QDs. (d) HR-TEM image of CdTe QDs adsorbed on surface of UCNPs.

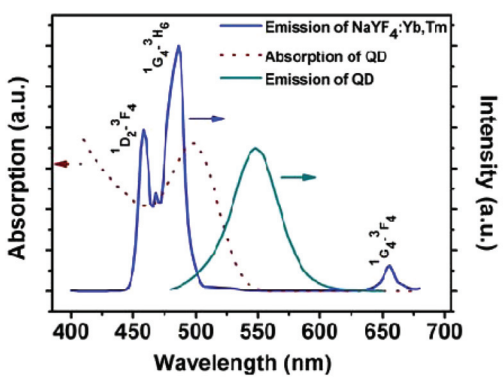

Fig. 2 Emission (blue line) spectrum of $NaYF_4$:Yb,Tm UCNPs; absorption (red dashed line) and emission (green solid line) spectra of CdTe QDs.

sufficient conditions for UCNP→CdTe QD non-radiation energy transfer or radiation energy transfer (energy reabsorption) to take place because the donor upconverted green luminescence overlaps with the strong absorption band of the acceptor. Another important reason that CdTe was selected as the FRET acceptor is that the UCNPs can be excited using an NIR laser at 980 nm where CdTe cannot be photoexcited, thereby avoiding CdTe excitation by external light and eliminating luminescence background interference.

The corrected emission spectra of Tm^{3+} ions *versus* the concentration of QDs in the $NaYF_4$:Yb,Tm/CdTe QDs mixture solution under the excitation of 980 nm laser diode are shown in Fig. 3(a) and the original emission spectra are shown in Fig. S1.† With the addition of the QDs, the concentration of the UCNPs decreased, leading to decreased emission intensity, so the spectra were corrected *via* $I = I_0/[Q]$, where I and I_0 represent the intensity of the corrected and origin spectra, respectively, and [Q] stands for UCNP concentration. In Fig. 3, it can be seen that the emission band of the QDs gradually increases with QD addition, while the blue emission at 430–520 nm of Tm^{3+} decreases. The red emission at 630–680 nm is almost unchanged. It should be noted that in the existence of the QDs, if only the non-radiation energy transfer from Tm^{3+} to the QDs happens, the intensity ratio of the $^1G_4$–$^3H_6$ at 484 nm and $^1G_4$–$^3F_4$ at 653 nm should be unchanged, since both the transitions originate from the same excited state. Therefore, it is suggested that in the existence of the QDs, the radiation energy transfer also happens from Tm^{3+} to the QDs – that is, the $^1G_4$–$^3H_6$ emission of Tm^{3+} is reabsorbed by the QDs, leading to the variation of the intensity ratio of $^1G_4$–$^3H_6$ (484 nm) to $^1G_4$–$^3F_4$ (653 nm) (The detailed mechanism is as shown in Fig. 4).

To further confirm the FRET process, the dynamic $^1G_4$–$^3H_6$ of Tm^{3+} transition processes with different QD concentrations were investigated. All the dynamic curves exhibited the same trends, namely, after an initial rise, the intensity of luminescence reached a maximum and then exponentially decayed (as shown in the inset). The curves can be well fitted by the following equation:[30]

$$I(t) = I_D e^{-t/\tau_D} - I_R e^{-t/\tau_R} \quad (2)$$

where τ_D and τ_R represent the decay and rising time constants, respectively, and I_D and I_R are both the positive constants. Note that the rising time constant τ_R is related to the energy transfer rate from Yb^{3+} to Tm^{3+}, while τ_D depends strongly on the depopulation process of the emission level. The constants of the rising and decay time as a function of the amount of QDs are shown in Fig. 3(b). It can be clearly seen that with the increasing concentration of QDs from 0 to 54%, the decay time for $^1G_4$–$^3H_6$ transition of Tm^{3+} decreases from 263 to 209 μs, which is evidence for the non-radiation energy transfer from $^1G_4$ of Tm^{3+} to the QDs. The rising time remains almost unchanged with concentration variation, which means no influence on the energy transfer process from Yb^{3+} to Tm^{3+} due to QD appearance. The inset shows the UCL dynamic curves for the $^1G_4$–$^3H_6$ transition of Tm^{3+} under 980 nm excitation in the presence and absence of QDs. The energy transfer efficiency from $^1G_4$ of Tm^{3+} to the QDs can be calculated as follows:[31]

$$\eta = 1 - \tau'_D/\tau_D \quad (3)$$

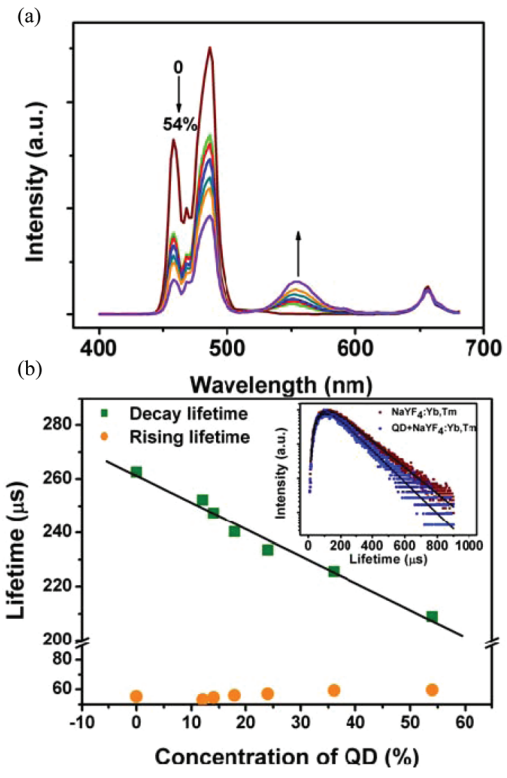

Fig. 3 (a) Revised FRET spectra with different QD concentrations of mixture solution. (b) Rising and decay lifetime constants of $^1G_4$ of Tm^{3+} at different QD concentrations (inset: dynamic curves of $^1G_4$–$^3H_6$ of Tm^{3+} transition in presence and absence of QDs).

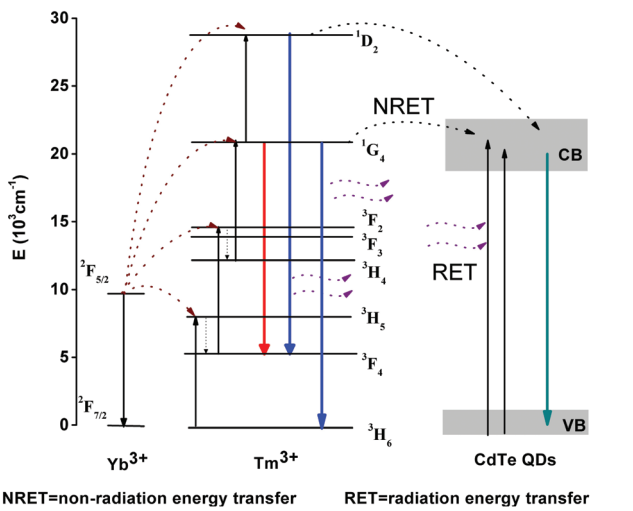

Fig. 4 Energy transfer upconversion processes from $NaYF_4$:Yb,Tm UCNPs to CdTe QDs.

where $\tau'D$ and τD represent the decay lifetime of $^1G_4$ level of Tm^{3+} in the presence and absence of QDs, respectively. According to the equation, the energy transfer efficiency is 20.8% when the QD concentration is 54%. It should be noted that there were no large aggregates during the mixing process with the increasing QD concentration, as seen in the photograph of the UCNP and QD complex (QD concentration is 54%; Fig. S2†).

The observed energy transfer upconversion processes are schematically illustrated in Fig. 4; the higher energy levels of Tm^{3+} ($^1D_2$, $^1G_4$) are populated through a four-photon process, and a three-photon process under 980 nm excitation. Energy-level spacing fits the energy gap between the conduction band (CB) and valance band (VB) of the CdTe QDs. The energy is transferred either by non-radiation or radiation mechanisms. Based on these results, we confirmed that both mechanisms were present.

3.3. Fluorescence response characteristics of FRET probe for Pb^{2+} detection

The principle of upconversion FRET lead-ion detection by employing UCNPs as energy donors and QDs as an energy acceptor is illustrated in Scheme 1. With the addition of QDs to the UCNPs, excitation of PEI-capped $NaYF_4$:Yb^{3+},Tm^{3+} UCNPs triggers energy transfer (ET) from Tm^{3+} to TGA-capped CdTe QDs within a given proximity through electrostatic interaction, and resulted in emission from QDs at 550 nm, and the weakening emission of Tm^{3+}. The TGA capping layer was crucial for QD luminescence efficiency and water stability. TGA capping was preferentially displaced from the surface of the QDs upon binding of Pb^{2+} ions. Displacement of TGA capping consequently created imperfections on the QD surface, resulting in fluorescence quenching. Thus, after adding the Pb^{2+} ions, the surface state of TGA-capped CdTe QDs changed with the addition of Pb^{2+}, leading to fluorescence quenching.[32]

To evaluate the sensitivity of this method, the fluorescence intensities of PBS buffer containing UCNPs, QDs and different amounts of Pb^{2+} were monitored. The extent of fluorescence quenching of QDs was dependent on Pb^{2+} concentration level, as shown in Fig. 5(a). The fluorescence quenching is best described by the Stern–Volmer equation:[11]

$$F_0/F = 1 + K[Q] \quad (4)$$

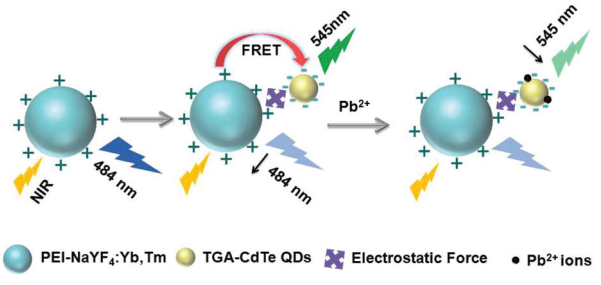

Scheme 1 Principle of upconversion lead-ion FRET detection by employing UCNPs as donor and QDs as acceptor.

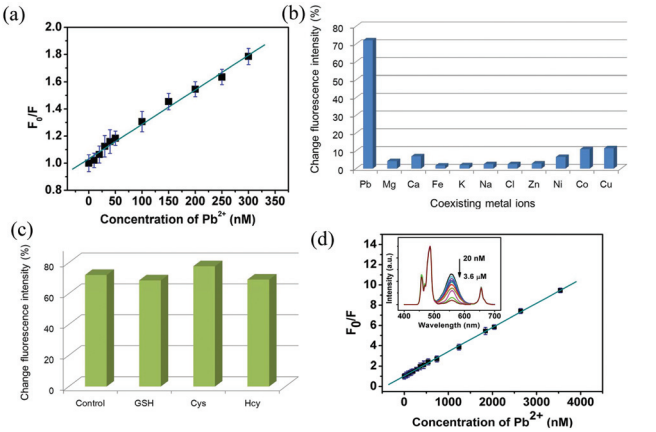

Fig. 5 (a) Fluorescence intensity of FRET sensor as a function of concentration of Pb^{2+} concentration detected in the buffer. (b) Detection selectivity for Pb^{2+}. Concentrations of all ions were 1 μM. (c) Detection of Pb^{2+} in absence and presence of interference in human serum, including GSH, Cys, and Hcy. (d) Fluorescence intensity of FRET sensor as a function of Pb^{2+} concentration detected in human serum (inset: FRET spectra of bioassay experiments detected in human serum with addition of various Pb^{2+} concentrations).

where F_0 and F are the fluorescence intensities of QDs in the absence and presence of Pb^{2+}, respectively, [Q] is the lead-ion concentration, and K_{SV} is the Stern–Volmer constant. The calibration plot showed a good linear relationship in the 20–300 nm range (R = 0.994), and K_{SV} was found to be 2.54 μM^{-1}.

To estimate the selectivity of the FRET probe for lead detection, Mg^{2+}, Ca^{2+}, Fe^{2+}, K^+, Na^+, Cl^-, Zn^{2+}, Cu^{2+}, Ni^{2+}, and Co^{2+} were investigated along with Pb^{2+}. As shown in Fig. 5(b), only Pb^{2+} led to a dramatic change of fluorescence intensity, and no significant fluorescence intensity variation was found with the presence of other ions. Selectivity coefficients, defined as the electrode response ratio caused by interfering ions and target ions, are shown in Table S1.† Interfering ions exhibited low selectivity coefficients in the range of 0.024–0.159. These results clearly demonstrated the great selectivity of the biosensor for the target ion. Because interference from glutathione (GSH), cysteine (Cys) and homocysteine (Hcy) in human serum may influence Pb^{2+} detection, the anti-interference performance of the biosensor was measured. Fig. 5(c) shows the response of 1 μM Pb^{2+} in the absence (control) and presence of 1 mM GSH, Cys, Hcy in the buffer, respectively. Adding each material did not significantly influence Pb^{2+} detection, which illustrates the biosensor's excellent anti-interference performance.

Because of superior sensitivity, selectivity, and anti-interference performance of our FRET probe in the buffer solution, we explored its capability to detect Pb^{2+} in human serum. As shown in the Fig. 5(d) inset, upon addition of Pb^{2+} ions, the emission from 500 to 600 nm of QDs decreased continuously in intensity, but without a peak shift. Meanwhile, the emission intensity of Tm^{3+} in the range of 400–500 nm and 600–700 nm did not change. The calibration plot of F_0/F *versus* Pb^{2+} concentration showed a good linear relationship in the 20–3600 nm range, as shown in Fig. 5(d). The plots are well described by

the Stern–Volmer equation (R = 0.996), and K_{SV} was found to be 2.48 μM^{-1}. The results were similar to those detected in the PBS buffer. The theoretical detection limit was evaluated using $3\sigma/S$ and calculated to be 80 nm, where σ represents the standard deviation of the blank signal. The σ can be calculated as

$$\sigma = \sqrt{\frac{\sum(F_n - \bar{F})^2}{n}},$$

where F_n represents the luminescence intensity for the nth time, F represents the average value of the luminescence intensity for multiple measurements, and S is the slope of the calibration plot. The U.S. Environmental Protection Agency (EPA) sets the safety limit of lead in the blood as 100 ppb (480 nm). As soon as the content of lead exceeds the standard, it can be detected by our system.

Various sensing strategies with chemically modified QD hybrid structures have been recently developed for sensing metal ions in aqueous solution.[29] To confirm that the proposed method was superior to the probe, which used only QDs for lead-ion detection in human serum, control experiments were carried out.

To evaluate detection sensitivity based on QDs in the buffer, the fluorescence intensities of PBS solutions containing QDs and different amounts of Pb^{2+} were monitored.

Upon the addition of Pb^{2+}, the fluorescence intensities of CdTe QDs were continuously decreased with the increase of Pb^{2+} concentration, as shown in Fig. 6 inset. The calibration plot of F_0/F *versus* Pb^{2+} concentration showed a good linear relationship in the range of 20–3600 nm. The probe based on QDs exhibited good performance of lead detection in the PBS buffer.

The emission spectra of QDs, the serum, and the mixture of QDs and serum under the excitation of 480 nm were measured. In Fig. 7 (left), it can be seen that the emission band of the QDs was located at 550 nm, and then blueshifted to 535 nm after serum was added to the QDs. The phenomenon was attributed to the influence of serum emissions at 515 nm under excitation of 480 nm. The serum emission is caused mainly by porphyrin, serum proteins, and carotenoids, as reported previously.[16]

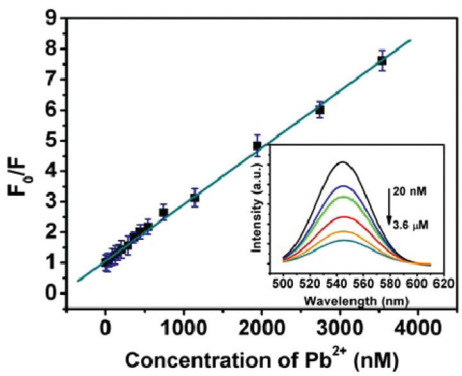

Fig. 6 Fluorescence intensity of QD-based sensor as a function of Pb^{2+} concentration detected in buffer (inset: fluorescence spectra of QDs with addition of various Pb^{2+} concentrations).

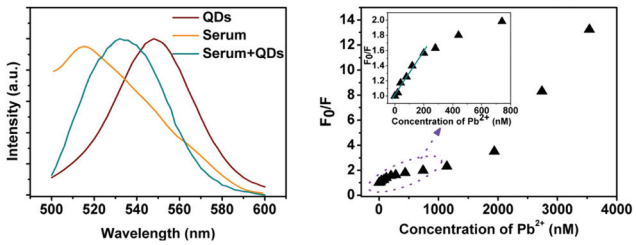

Fig. 7 Emission spectra of QDs (red line), serum (yellow line), and serum with QDs (green line) excited with 480 nm (left). Fluorescence intensity of QD-based sensor as a function of Pb^{2+} concentration detected in human serum (right).

Table 1 Pb^{2+} limit of detection (LOD) and linear range of six fluorescence sensors

QDs	Capping ligand or coating	Range (nM)	LOD (nM)	Ref.
CdTe	TGA	20–3600	80	This work
CdZnSe	GSH	5–20 000	20	11
CdTe	TGA	2000–100 000	270	12
CdTe	TGA	1.96–25.9	4.7	13
CdSe	DAB	10 000–150 000	60 000	14
CdSe/CdS	XO	50–6000	20	15

The capability of QDs to detect Pb^{2+} in serum was also explored, as exhibited in Fig. 7(b). As seen in the inset, the calibration plot of F_0/F *versus* Pb^{2+} concentration showed relatively good linearity at low concentrations of Pb^{2+} (20–200 nm); however, the calibration plot of F_0/F *versus* Pb^{2+} concentration showed poor linearity at the high concentrations (200–3600 nm). We considered that the luminescence of QDs gradually weakened with the adding of the lead, and the luminescence of the serum affected the whole intensity in high concentration of Pb^{2+}.

Compared to five other reported methods based on QDs, the proposed method shows better linear range and sensitivity, as shown in Table 1. All five methods detected lead ions in aqueous solution rather than in human serum. Autofluorescence of proteins in serum must be considered in further development lead-ion sensors. In 2013, Chung *et al.* reported a nuclease-resistant DNA aptamer on gold nanoparticles for Pb^{2+} detection in human serum.[1] The use of AuNP-conjugated aptamers made it possible to detect Pb^{2+} as low as 5 nm, which was lower than the detection limit of our system. However, the DNA aptamer must be subjected to complex chemical modification by Au nanoparticles to enhance its resistance to damage from nuclease. The system we established is a comparatively facile method to detect lead ions in human serum.

4. Conclusions

In conclusion, we developed a new type of lead biosensor based on FRET from UCNPs to QDs, which overcomes the lack

of NIR-excitable probes for lead ions. The sensor can be used for lead-ion sensing both in the PBS buffer and in serum with comparable performance, proving that the biosensor is capable of overcoming self-luminescence from serum excitation due to visible light. When applied to detect lead ions in human serum, the sensor had a good linear relationship (R = 0.996), and a low detection limit (80 nm), thereby easily detecting the 480 nm safety limit of lead in the blood. Thus, the sensor we designed has great potential for applications in lead detection in biological and analytical fields.

Acknowledgements

This work was supported by the Major State Basic Research Development Program of China (973 Program, 2014CB643506), National Natural Science Foundation of China (grants 11374127, 11304118, 61204015, 81201738, 81301289, 61177042, and 11174111), Program for Chang Jiang Scholars and Innovative Research Team in University (IRT13018), and Graduate Innovation Fund of Jilin University (project 2014094).

Notes and references

1 C. H. Chung, J. H. Kima, J. Jung and B. H. Chung, *Biosens. Bioelectron.*, 2013, **41**, 827.
2 D. I. Bannon, C. Murashchik, C. R. Zapf, M. R. Farfel and J. J. Chisolm Jr., *Clin. Chem.*, 1994, **40**, 1730.
3 S. C. K. Shum, H. M. Pang and R. S. Houk, *Anal. Chem.*, 1992, **64**, 244.
4 Y. Bonfil and E. Kirowa-Eisner, *Anal. Chim. Acta*, 2002, **457**, 285.
5 T. Sokalski, A. Ceresa, T. Zwickl and E. Pretsch, *J. Am. Chem. Soc.*, 1997, **119**, 11347.
6 J. Y. Kwon, Y. J. Jang, Y. J. Lee, K. M. Kim, M. S. Seo, W. Nam and J. Yoon, *J. Am. Chem. Soc.*, 2005, **127**, 10107.
7 P. Chen, B. Greenberg, S. Taghavi, C. Romano, D. Lelie and C. He, *Angew. Chem., Int. Ed.*, 2005, **44**, 2715.
8 J. W. Liu and Y. Lu, *J. Am. Chem. Soc.*, 2003, **125**, 6642.
9 C. T. Chen and W. P. Huang, *J. Am. Chem. Soc.*, 2002, **124**, 6246.
10 L. Wang, C. J. Yang, C. D. Medley, S. A. Benner and W. H. Tan, *J. Am. Chem. Soc.*, 2005, **127**, 15664.
11 E. M. Ali, Y. G. Zheng, H. H. Yu and J. Y. Ying, *Anal. Chem.*, 2007, **79**, 9452.
12 H. M. Wu, J. G. Liang and H. Y. Han, *Microchim. Acta*, 2008, **161**, 81.
13 W. Y. Zhong, C. Zhang, Q. Gao and H. Li, *Microchim. Acta*, 2012, **176**, 101.
14 M. Algarraa, B. B. Camposb, B. Alonsoc, M. S. Mirandaa, Á. M. Martínezc, C. M. Casadoc and J. C. G. E. Silvab, *Talanta*, 2012, **88**, 403.
15 Q. Zhao, X. L. Rong, L. Chen, H. B. Ma and G. H. Tao, *Talanta*, 2013, **114**, 110.
16 J. Yu, J. W. Meng, Y. Li, J. Ma and R. E. Rong, *Spectrosc. Spectral Anal.*, 2004, **24**, 981.
17 J. L. Liu, Y. Liu, Q. Liu, C. Y. Li, L. N. Sun and F. Y. Li, *J. Am. Chem. Soc.*, 2011, **133**, 15276.
18 S. Xu, W. Xu, Y. F. Wang, S. Zhang, Y. S. Zhu, L. Tao, L. Xia, P. W. Zhou and H. W. Song, *Nanoscale*, 2014, **6**, 5859.
19 R. Gill, M. Zayats and I. Willner, *Angew. Chem., Int. Ed.*, 2008, **47**, 7602.
20 M. Y. Gao, C. Lesser, S. Kirstein and H. Mohwald, *J. Appl. Phys.*, 2000, **87**, 2297.
21 A. Gupta, V. Parikh and A. D. Compaan, *Sol. Energy Mater. Sol. Cells*, 2006, **90**, 2263.
22 C. Wang, Q. Ma, W. C. Dou, S. Kanwal, G. N. Wang, P. F. Yuan and X. G. Su, *Talanta*, 2009, **77**, 1358.
23 F. Wang and X. G. Liu, *Chem. Soc. Rev.*, 2009, **38**, 976.
24 J. Zhang, B. Li, L M. Zhang and H. Jiang, *Chem. Commun.*, 2012, **48**, 4860.
25 Y. Liu, M. Chen, T. Y. Cao, Y. Sun, C. Y. Li, Q. Liu, T. Yang, L. M. Yao, W. Feng and F. Y. Li, *J. Am. Chem. Soc.*, 2013, **135**, 9869.
26 F. Wang and X. G. Liu, *J. Am. Chem. Soc.*, 2008, **130**, 5642.
27 H. Zhang, Z. Zhou and B. Yang, *J. Phys. Chem. B*, 2003, **107**, 8.
28 W. W. Yu, L. Qu, W. Guo and X. Peng, *Chem. Mater.*, 2003, **15**, 2854.
29 Y. Kobayashi, L. Y. Pan and N. Tamai, *J. Phys. Chem. C*, 2009, **113**, 11783.
30 S. Xu, W. Xu, B. Dong, X. Bai and H. W. Song, *J. Appl. Phys.*, 2011, **110**, 113113.
31 A. Bednarkiewicz, M. Nyk, M. Samoc and W. Strek, *J. Phys. Chem. C*, 2010, **114**, 17535.
32 B. J. Fuhr and D. L. Rabenstein, *J. Am. Chem. Soc.*, 1973, **95**, 6944.